EEET ECOLOGICAL ENGINEERING & ENVIRONMENTAL TECHNOLOGY

Ecological Engineering & Environmental Technology, 2026, 27(4), 1–18
https://doi.org/10.12912/27197050/218414
ISSN 2719–7050, License CC-BY 4.0

Received: 2026.02.18
Accepted: 2026.03.16
Published: 2026.04.01

Simulating the impact of climate and land cover changes on river discharge in the Maros watershed

Muhammad Dandy Rachmat Ramadhan[1], Andang Suryana Soma[2*], Roland A. Barkey[2]

[1] Forestry Master Program, Faculty of Forestry, Hasanuddin University, 90245, Makassar, Indonesia
[2] Department of Forestry, Faculty of Forestry, Hasanuddin University, 90245, Makassar, Indonesia
* Corresponding author's e-mail: s_andangs@unhas.ac.id

ABSTRACT

The Maros watershed is a rapidly urbanizing tropical karst region experiencing severe land degradation and annual flooding. To address these extreme hydrological risks, this study proposes an integrated climate-land cover dynamic simulation framework utilizing the soil and water assessment tool (SWAT) to quantify the impact of each driver on extreme discharge dynamics. According to the results of the analysis of precipitation and temperatures from 1983–2023, there was a fluctuating trend in annual precipitation, with an average of 1,979.53 mm/year (the highest in January, with a value of 370.16 mm/month), while the temperature was 26.27 °C. However, the results of the 2064 projection show that the trend of rainfall increases in rainy months by between 1% and 4% and decreases in dry months by 32%. In the land cover area projected by 2064, land degradation occurs, where the area of secondary forests is projected to decrease by 50.41 ha/year (382.18 ha/year from 2014–2023), as well as the expansion of agricultural land (26.25 ha/year for agriculture/crop land and 0.54 ha/year for paddy areas) and settlements (24.11 ha/year). The results of the SWAT simulation describe a highly sensitive (striking) flow characteristic where extreme intense rains occurred on December 7, 2021, resulting in simulated maximum flows of 1,206 m^3/s in sub watershed 6, 618.70 m^3/s in sub watershed 23 and 289.80 m^3/s in sub watershed 46. In terms of the projection, the maximum flow occurred on February 13, 2064, with flows of 184.10 m^3/s in sub watershed 6, 133 m^3/s in sub watershed 23, and 79.40 m^3/s in sub watershed 46. The resulting flow value represents a rapid response between the extreme precipitation event and land cover change for the discharge surge. The results of the validation of the best SWAT model at the Lekopaccing Dam revealed satisfactory performance, with a Nash-Sutcliffe (NSE) value of 0.75.

Keywords: Maros watershed, land cover change, climate change, discharge, SWAT model.

INRODUCTION

Since the 1980s, Mamminasata, which includes Makassar city, Maros Regency, Gowa Regency, and Takalar Regency, has transformed into a metropolitan area in Eastern Indonesia (Sulmiah et al., 2019). Makassar serves as the main growth hub (metropolitan core), with its influence extending to the surrounding regions. Maros Regency, as one of the buffer regencies (metropolitan periphery) in the Mamminasata area, contributed to the highest economic growth of the other regencies, with a primary economy of 25.33% (agricultural), a secondary economy of 20.15% (industrial management activities), and a tertiary economy of 54.50% (trade and provision of services) from 2015–2020 (Yanuar et al., 2023). This economic growth cannot be separated from the role of its natural landfill, namely, the Maros watershed, which functions as a critical ecological and economic support system, supplying water for domestic consumption, industrial operations, transportation infrastructure (National Strategic Project/PSN of the Makassar–Parepare Railway and Sultan Hasanuddin International Airport), agriculture, irrigation, and strategic tourism objects (Djafar and Faisal, 2019; Hayati and Wakka, 2016; Suhairin, 2020). Therefore, the linkage

between the Maros watershed and the Mamminasata metropolitan area supports economic activities in terms of water quality, land use, and productivity (Rajaei et al., 2016; Surya et al., 2021; Zhong et al., 2022).

However, an important ecological function of the region, the Maros watershed is now experiencing severe degradation because of changes in land cover and the global climate. Alterations in land cover and climate significantly influence the hydrological cycle of a watershed. These changes are based on high agricultural activity, urban area expansion, and significantly high deforestation rates (Malede et al., 2023). High agricultural activity and land expansion encourage irrigation, which causes changes in river flow patterns by decreasing the base flow and increasing the maximum flow due to reduced natural vegetation (Liu et al., 2020). Furthermore, increased urban development, the construction of river-bordered structures, and the construction of zones that ignore flood zoning have led to increased peak flows and impermeable surfaces, thus exacerbating the risk of flooding (Dwivedi et al., 2024; Knighton et al., 2017; Talib and Randhir, 2017). The implications of this phenomenon include an increase in temperature and changes in precipitation patterns, an increase in the volume of surface runoff, changes in the intensity of evapotranspiration, and a significant increase in river flow (Hyandye et al., 2018; Kumar et al., 2022). Combined with shifting precipitation patterns, these transformations cause problems, such as annual flooding, river sedimentation, and damage to karst ecosystems. The annual overflow of the Maros watershed poses problems for transportation, economic and social connectivity (Pregnolato et al., 2017). These transformations are expected to intensify under future climate scenarios, potentially amplifying hydrological extremes, and require an urgent assessment of the impact of changes in hydrological responses and fluctuations derived from extreme flows (Wldmchel and Osore, 2025). However, three major research gaps remain, particularly in rapidly urbanizing tropical watersheds: (1) there is limited use of combining changing land cover and adjusted climate predictions in a single water model; (2) there is insufficient research on how much climate change and land use change impact extreme discharge dynamics; and (3) tropical karst-influenced watersheds are not often included in long-term studies on climate and water flow, even though they have complex and sensitive runoff patterns.

Predicting discharge amid changing environmental and climatic conditions poses considerable challenges in complex hydrological cycles. The variability of input meteorological data, changes in land use/land cover, and other watershed features require a modeling approach that can accurately capture spatial and temporal diversity (Cordeiro et al., 2017; Hasan and Pradhanang, 2017). It is important to observe the extent to which the existing change process is affected by simulating hydrological processes via models. Water and soil assessment tools (SWAT) have been used in several studies to simulate hydrologic cycles because of their ability to calculate surface runoff, infiltration, evapotranspiration, and discharge dynamics (Akoko et al., 2021). SWAT models have been widely used to simulate hydrological processes, considering the effects of land management, climate change and adaptation strategies, and water resource planning (Wang et al., 2019). Owing to this capability, SWAT is considered a computationally efficient prediction model for predicting river flow on the basis of meteorological, topographic, soil, and land cover data (Akoko et al., 2021; Huang et al., 2024). Moreover, SWAT simulates daily, monthly, or annual river discharges (Golmohammadi et al., 2014; Moura et al., 2025).

To address the identified research gaps, this study aims to develop and implement a comprehensive simulation framework. This framework will integrate dynamically projected land cover change, bias-corrected climate projections, and distributed hydrological modeling using SWAT. Two programs, LanduseSim and SiBias, were used in this study for the projection scenarios. LanduseSim is an algorithm that uses a cellular automata (CA) model to predict land cover, allowing users to control all spatial simulation procedures, such as growth targets and driving factors (Pratomoatmojo, 2018a). SiBias assists in processing climate projection data by extracting CMIP5 GCM data and bias-correcting climate data (Faqih, 2017). The primary scientific objective is to assess the relative and combined effects of climate variability and land cover change on discharge dynamics within a rapidly urbanizing tropical karst watershed. This study is specifically guided by the following research hypotheses: (1) anticipated land-cover degradation and urban expansion are expected to significantly increase peak discharge and decrease base flow, attributable to a reduction in vegetative buffering capacity and an increase in surface impermeability; (2)

bias-corrected climate projections, which indicate intensified wet-season rainfall and diminished dry-season precipitation, are predicted to amplify seasonal discharge variability; (3) the combined effects of land-cover change and climate variability are hypothesized to produce a non-linear amplification of extreme flow responses at the sub-watershed scale, surpassing the impact of each driver when acting independently; and (4) hydrological responses are anticipated to exhibit strong spatial heterogeneity, with sub-watersheds experiencing varying sensitivities depending on the intensity of land transformation and local physiographic characteristics.

MATERIALS AND METHODS

Research location

The Maros watershed is a basin with a strategic hydrological system in the Province of South Sulawesi, covering an area of 72,348.95 ha and extending from the upper parts of the karst and volcanic mountains to the lower coast of the Makassar Strait. Administratively, most of it belongs to Maros Regency, with an area percentage of 91.78% (geographical coordinates 119°55'45.79"–119°27'56.85" east longitude and 5°8'3.45"–5°1'33.45" south latitude). (Figure 1). As an integral part of the Mamminasata Metropolitan Area, it supports regional economic growth by providing ecosystem services for the agricultural, industrial, and national sectors, as well as for various National Strategic Projects (NSP). The unique biophysical characteristics of the region, with the predominance of karst landscapes as natural equators, make the hydrological system complex, and the challenge of the impact of the degradation of dynamic soil functions is expert pressure.

SWAT model

Developed under the auspices of the USDA's agricultural research service (ARS) by Dr. Jeff Arnold, SWAT is a modeling instrument designed specifically for watershed-scale hydrological analyses (Farzana et al., 2019). SWAT was designed to simulate the hydrological response to interventions in land use/cover patterns and climate change phenomena. The mechanism or workflow of this model involves dividing the

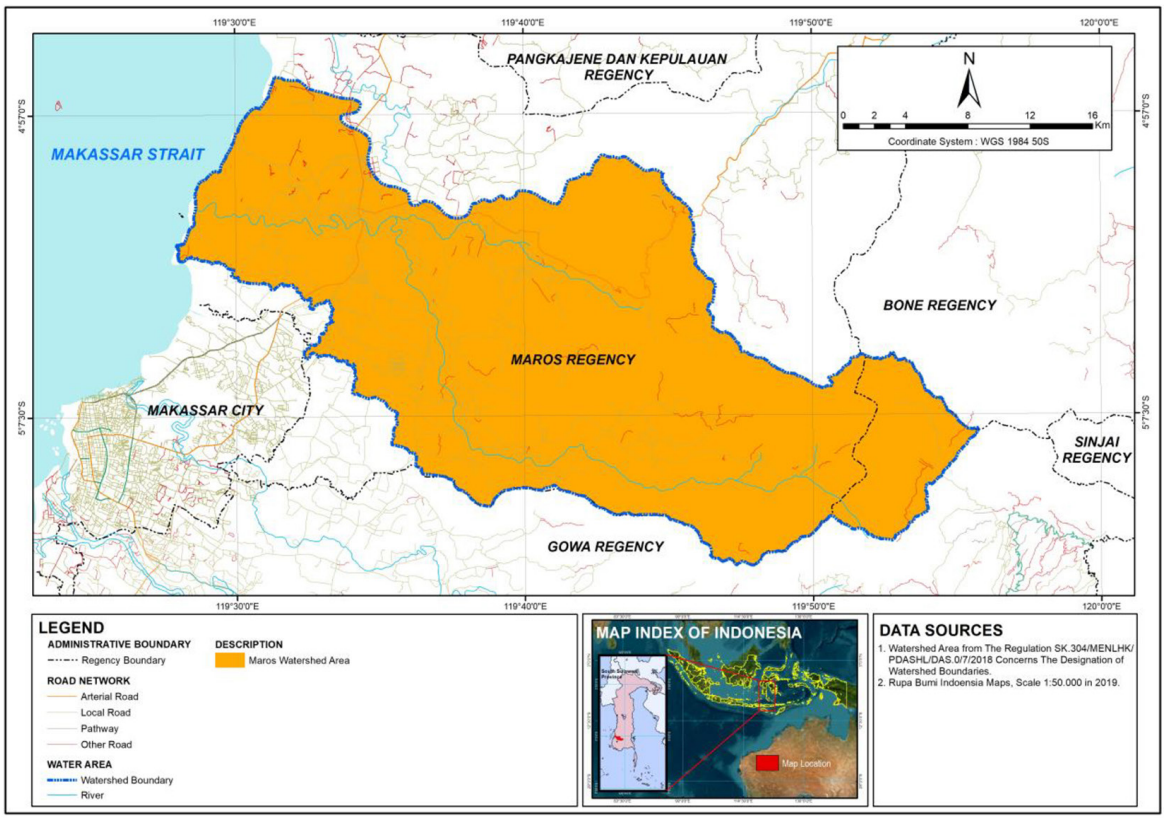

Figure 1. Research location

study area into sub watersheds and grouping them into hydrology response units (HRUs). The HRU is the result of the overlay of soil, slopes, and land cover (Xu et al., 2010). To produce comprehensive simulations at daily and monthly time intervals, the model requires climatological input data in the form of rainfall, temperature, relative humidity, wind speed, and solar radiation (Kibii et al., 2021) (Table 1).

Data preparation

Digital elevation model (DEM)

The DEM data were used in this study as the topographical basis for delineating the watershed and its sub watershed boundaries, forming river networks, and slope classification, which serves as the primary data for HRU formation.

Land cover

Land-cover maps were generated through the supervised classification of Landsat 8 imagery for the years 2014, 2019, and 2023. Multispectral composites were created utilizing bands 6–5–4 (SWIR1–NIR–Red), followed by pan-sharpening with the 15 m panchromatic band to enhance spatial detail. Land-cover change over the decade (2014–2023) was evaluated using a post-classification change detection approach. Change detection involves determining the rate of ground change at any time via remote sensing technology in a specific study area between two or more time periods (Soma and Kubota, 2017). Transitions among land cover categories were quantified by comparing classified maps from different years. The classification performance was assessed using a confusion matrix to calculate the overall accuracy and kappa coefficient, ensuring that only outputs meeting acceptable accuracy thresholds were retained for subsequent modeling.

LanduseSim software was utilized for future land-cover projections. LanduseSim is an algorithm that uses a cellular automata model to predict land use, allowing users to control spatial simulation procedures, such as growth targets and driving factors (Pratomoatmojo, 2018a, 2018b). The simulation incorporated four spatial driving factors: distance to primary roads, distance to secondary roads, distance to rivers, and distance to existing settlements. The existing 2023 land-cover data were codified as the baseline. All spatial datasets were converted into a 30 m raster format, as required by the cellular automata unit of analysis (Pratomoatmojo, 2018c).

Meteorological data

NASA's "The Modern-Era Retrospective Analysis for Research and Applications" (MERRA)-II climate data were used in this study because the completeness of the data was in line with the needs of the data in SWAT modeling, with a pixel resolution of 0.5° × 0.625° or 50 km (Gelaro et al., 2017). The data were downloaded based on the coordinates of the weather station, with a resolution of 14 km. This resolution was a result of the reduction in the GCM for the eastern archipelago of Indonesia (McGregor et al., 2016). The data collection years were 1983–2023 for climate change analysis with precipitation and temperature data and 2010–2023 for SWAT climate data on precipitation, temperature (maximum and minimum), solar radiation, humidity, and wind speed.

The climate change scenario in the Maros watershed was analyzed via the Statistical Bias Correction for Climate Scenarios (SiBiaS)

Table 1. Data used in SWAT modeling

No	Data	Type	Period	Source
1	Digital elevation model (DEM)	Raster – resolution 0.27 arcsecond (8.1 m)	2018	Ina Geoportal of the Geographic Information Agency (BIG) https://tanahair.indonesia.go.id/demnas/#/
2	Meteorological data	Tabular – daily with resolution 0.5° × 0.625° or 50 km	1983–2023	Climate data *"The Modern-Era Retrospective analysis for Research and Applications"* (MERRA) – II Nasa https://power.larc.nasa.gov/data-access-viewer/
3	Landsat-8 imagery	Raster – resolustion 30 m	2014, 2019, and 2023	United States Geological Survey (USGS) https://earthexplorer.usgs.gov
4	Soil data	Vector – scale 1:250,000	1984	*Landsystem* RePPProT and soil sampling
5	Observation discharge data	Daily	2010–2023	BBWS Pompengan Jeneberang

program, which helps to represent the output of the CMIP5 GCM data from the MERRA-2 data. With this application, CMIP5 absorbs the representative concentration pathway (RCP) scenario model. RCP is a term used in future climate scenarios to represent the range of radiative forcing values in climate models of 2.6 W/m^2, 4.5 W/m^2, 6 W/m^2, and 8.5 W/m^2. However, only a few GCM models can be represented for the Indonesian region, one of which is CSIRO-Mk3-6-0. CSIRO-Mk3-6-0 has very strong results in simulating climate change in the Indo-Pacific region, with an RCP of 4.5 W/m^2 (Rotstayn et al., 2012). Therefore, in this study, the CSIRO-MK3-6-0 scenario was applied.

Soil data

Soil data required for this study included soil type classification and soil physical and chemical property parameters. The soil classification and associated property data were obtained from the Regional Physical Planning Program for Transmigration (RePPProT) compiled by the National Coordinating Board for Survey and Mapping (Bakosurtanal) in 1987, at an original scale of 1:250,000. To improve spatial resolution for watershed-scale modeling, the dataset was adjusted to a scale of 1:50,000. Detailed soil information was further refined through a field-based soil survey, including soil sampling of individual land units (LU). A land unit is defined as a spatial area comprising soils with homogeneous or similar physical and chemical characteristics. In addition to RePPProT soil classifications, slope classes were incorporated to account for topographic influence on hydrological processes. These combined datasets provided the necessary input parameters for the subsequent SWAT hydrological modeling (Figure 2).

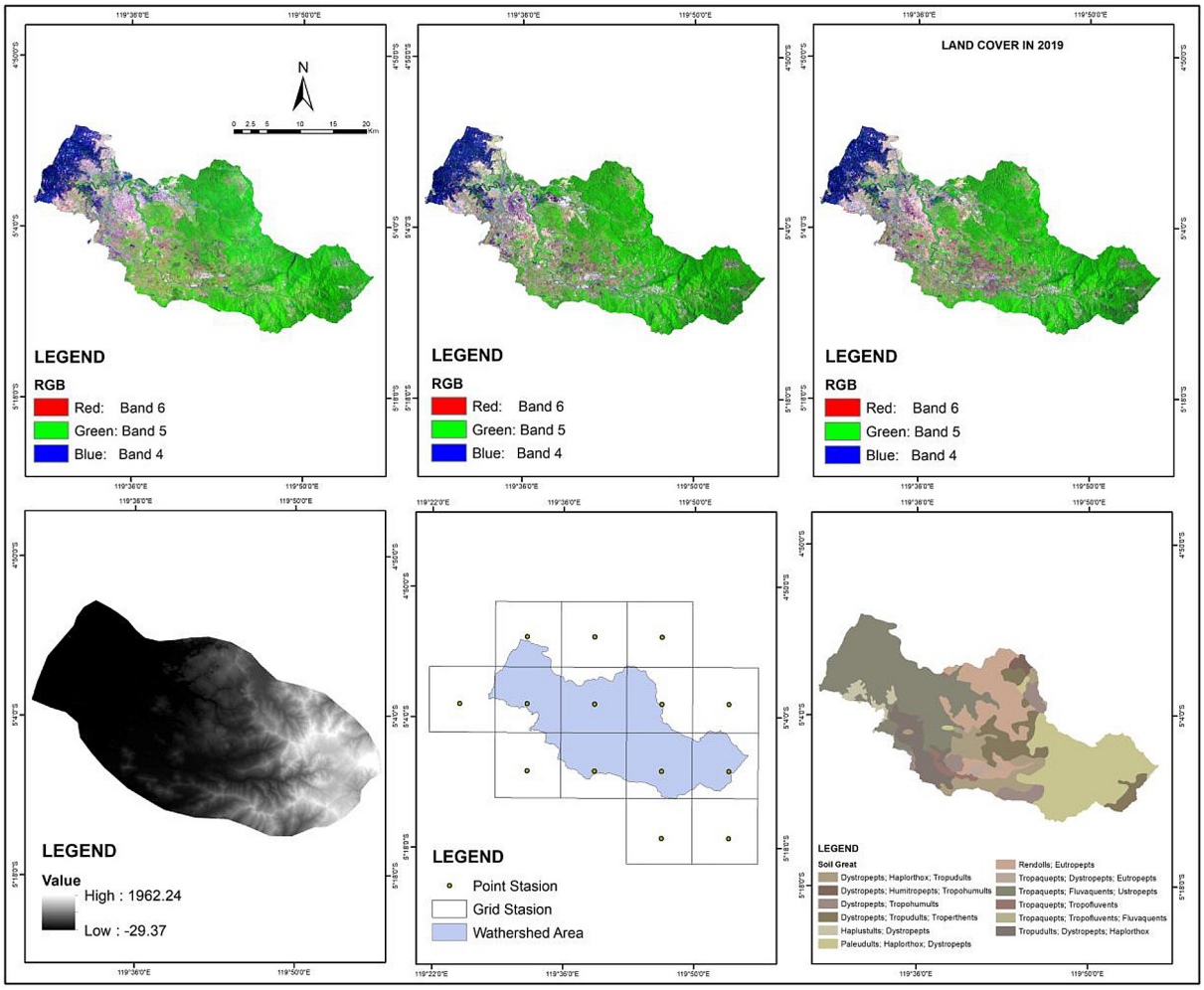

Figure 2. Spatial data preparation: a) Landsat 8 2014; b) Landsat 8 2019; c) Landsat 8 2023; d) DEM data; e) point station climate; f) soil map

Model setup

SWAT is processed through a GIS application, specifically ArcSWAT, which requires spatial data, both vector and raster data, and tabular data for the simulation. The spatial data consisted of digital elevation model (DEM), soil, and land cover data. Tabular data were presented in the form of climate data. The first phase involves delimiting the limits of the hydrographic watershed. At this stage, the information generated is presented in the form of watershed morphometry in the form of watershed boundaries, flow directions, flow accumulation, and stream outlets. It will also form another hydrographic sub watershed. The data required are DEM data and river lines (for burn-in DEMs). HRU formation is a unit or terrestrial unit with various elements formed from land cover map data, soil type maps, and terrain slope maps. Each HRU has the composition of the land cover, type of soil, and slope of each sub watershed. Climate data entry was performed by selecting the Write Input Tables menu by calling the weather generator data (WGN) file that had been previously transformed, that is, precipitation (pcp.txt), temperature (tmp.txt), solar radiation (solar.txt), relative humidity (rh.txt), and wind speed (wind.txt).

The simulation process can be performed after the data on HRU formation and climate are successfully obtained. This simulation was performed with the Run SWAT tool in the SWAT simulation menu by setting the time period, the SWAT version, and the amount of time data generated, that is, daily, monthly, or yearly. The SWAT model was then run to produce the hydrological conditions. The SWAT model is based on the principle of water balance (Xie and Zhu, 2022) and is expressed by the following algorithm:

$$S_t = S_0 + \sum_{i=1}^{t} \begin{pmatrix} RS_{day} - Q_{surf} - \\ -E_{act} - S_{seep} - Q_{gw} \end{pmatrix} \quad (1)$$

where: S_t represents the final soil water content (mm), S_0 represents the initial soil water content (mm), t represents time (day), RS_{day} represents daily rainfall (mm), Q_{surf} represents daily surface runoff (mm), E_{act} represents daily evapotranspiration (mm), S_{seep} represents daily percolation (mm), and Q_{gw} represents daily lateral flow (mm).

The simulation process can be divided into four models. Model 1 simulates 2014 land cover data with 2010–2014 climate data. In this model, a calibration review process is performed to help correct problems in the simulation results with the fitted value. The 2019 land cover model 2 with 2015–2019 climate data, 2023 land cover model 3 with 2020–2023 climate data, and 2064 projected land cover model 4 with 2064 climate data are used as validation models on the basis of the calibration results. The SWAT output has several file types (SWAT output files), and in this study, we focused solely on the RCH files. The RCH file contains the simulated data.

Model calibration and validation

The statistical methods used to calibrate and validate the model are the coefficient of determination (R^2) model and the Nash-Sutcliffe efficiency (ENS) model recommended by American Civil Engineers. The calibration stage was performed in SWAT-CUP by analyzing sensitive parameters that referenced observational downloaded data. The simulation used five parameters: R_CN2 (curve number), V_ALPHA_BF (baseflow alpha factor), V_GW_DELAY (groundwater delay), R_GWQMN (depth of the shallow aquifer needed to return the flow), and R_SURLAG (surface runoff delay coefficient). The Nash–Sutcliffe value (ENS) describes the level of correlation between simulation and observational data, where the index value is between 0 and 1. ENS model is used to evaluate the simulation outcome model. According to the NSE criteria, the simulation is considered decent if the NSE value is > 0.75, satisfactory if the NSE value is 0.36 < NSE < 0.75, and less feasible if the NSE value is < 0.36 (Upadhyay et al., 2022).

RESULTS AND DISCUSSION

Climate change

The results of the precipitation analysis of the Maros watershed from 1983–2023 (Figure 3) revealed a fluctuating trend. The average precipitation during this period was 1,979.53 mm/year, with the highest peak occurring in 1999 (3,440.69 mm) and the lowest occurring in 2005 (1,237.10 mm). The data show that from the 1990s to the 2000s, the highest precipitation often

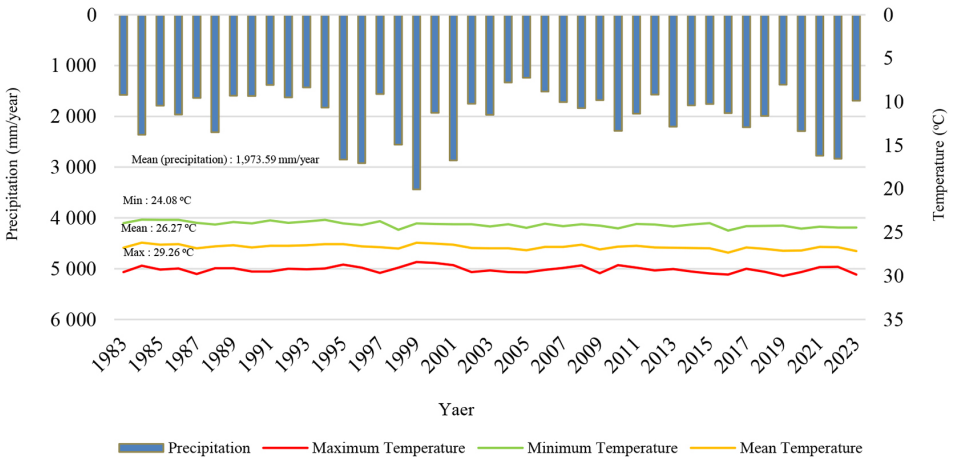

Figure 3. Annual climate trends (precipitation and temperature) in the Maros watershed (1983–2023)

occurred and began to decline in the 2010s. The following period until 2023 will increase again. Moreover, the relative temperature was stable in the range of 24.08–29.26 °C at the maximum and minimum values, with an average of 26.27 °C.

The climate variability that occurs is inversely proportional to the results of the 40-year scenario in the Maros Basin (Figure 4). A significant warming trend in air temperature was identified, characterized by an average temperature of 27.74 °C and an overall maximum value of 30.32 °C. This resulted in an average decrease in rainfall of 1,945.52 mm/year or 28.07 mm/year, or approximately -1.07%. Contrasting results were observed in the change delta based on the CSIRO climate model MK-3.6.0. During the rainy season (December, January and February), the model projected greater rainfall than did the observational data. This can be seen in the increase in rainfall of >1–4%, indicating an increase in rainfall intensity and implications for an increase in peak discharge. In contrast, the dry season period (June, July and August) showed a significant decrease. The largest decline occurred in August, with a reduction of 32.02%, indicating extreme drought conditions and a deficit in water availability in the Maros watershed in the middle of the year. The transition period between March–May and September–November tends to vary (Figure 5).

Existing climatic fluctuations then cause La Niña. La Niña has an impact on increased rainfall through changes in sea surface temperature in the Pacific Ocean, which affect atmospheric circulation and water vapor distribution. This causes increased rainfall, especially in areas easily affected by ENSO (El Nino–South Oscillation). Specifically, La Niña, which occurs in Indonesia, causes extreme precipitation, such as the number of consecutive days of precipitation, and tends to lead

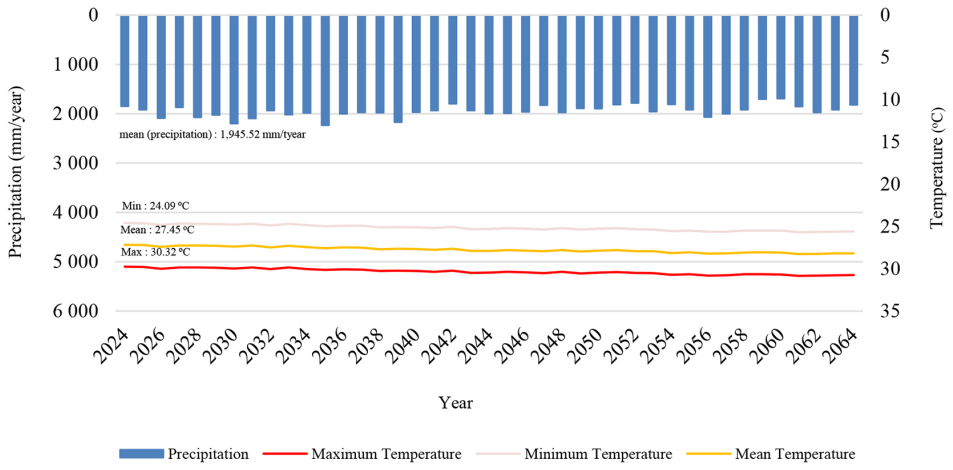

Figure 4. Trends of annual climate scenarios (precipitation and temperature) in the Maros Watershed (2024–2064)

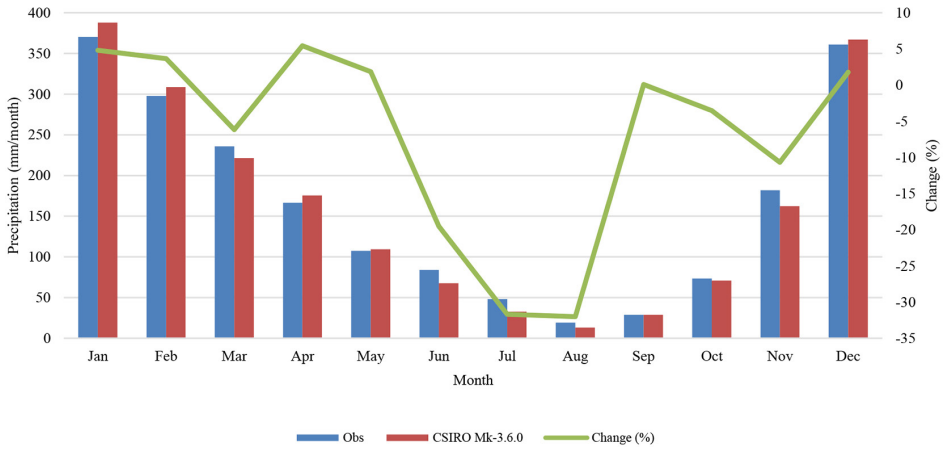

Figure 5. Percentage change in the percentage of rainfall in the Maros watershed in 2064

to extreme weather anomalies and drought conditions due to El Niño. Therefore, La Niña events are often associated with high precipitation and extreme hydrometeorological events, such as flooding, in various regions of the world (Huang et al., 2024; Supari et al., 2017; Ummenhofer et al., 2015).

According to the results of the CSIRO, Mk-3.6.0. In the climate model, climate change is indicated by a change in the hydrological cycle characterized by a decrease in the intensity of annual rainfall that coincides with an increase in the average temperature. The CSIRO-Mk3-6-0 model tends to project drier conditions in some regions of southern Indonesia (including South Sulawesi) below RCP 4.5, which is consistent with the drying trend in the maritime continent projected by the CORDEX-SEA and CMIP5 studies (Aprizal and Meris, 2020; Tangang et al., 2020). The increase in temperature has a dual hydrometeorological impact, specifically evapotranspiration, which affects the water deficit in the dry season and prolongs the duration of the drought, as does the occurrence of extreme rainfall anomalies in certain months that can cause flash floods. These complex climate interactions are giving rise to increasingly dynamic hydrological responses, especially when juxtaposed with changes in land cover patterns within watersheds (Farjad et al., 2016; Malede et al., 2023; Mollel et al., 2023) (Figure 6).

Land cover changes

The results of the ground cover accuracy test yielded accurate results, with overall accuracies of 98.10% (2014), 98.60% (2019), and 98.17% (2023) and kappa accuracies of 97.69%, 98.31%, and 97.80%, respectively. Data verification in 2014 and 2019 used high-resolution imagery from Google Earth Pro as a reference, whereas validation in 2023 was performed through direct field surveys. (Islami et al., 2022; Tilahun and Teferie, 2015). These results show that the precision value has a high accuracy rate of at least 80% for the overall and kappa data (Mathewos et al., 2022).

According to Table 2, the analysis of the last ten years revealed a massive transition in land use in the Maros watershed, dominated by the conversion of forest cover into agricultural areas and built-up land. The dryland secondary forest class recorded the highest deforestation rate, with a cumulative area loss of 3,439.61 ha (382.18 ha/year). The downward trend is constant at 34.86% in 2023, indicating fairly high pressure in the upstream and midstream basins.

The growth of urbanized areas of settlements shows a very aggressive trend, with the addition of 1,300.32 ha (144.48 ha/year), indicating intensive urbanization. This trend correlates with population pressures and the development of metropolitan areas, which hydrologically implies the expansion of impermeable layers and an increase in the runoff coefficients. In addition to settlements, dryland agriculture has also experienced a massive expansion of 2,589.71 ha (287.75 ha/year), increasing its domain of use to 13.26% by 2023. In contrast, mixed agriculture/agroforestry and ponds decreased by 1,295.88 ha and 278.54 ha, respectively. The paddy area showed a moderate increase of 1,046.36 ha, reinforcing its position as the second highest coverage area (19.36%). These data show a focus or intensification of agricultural land use.

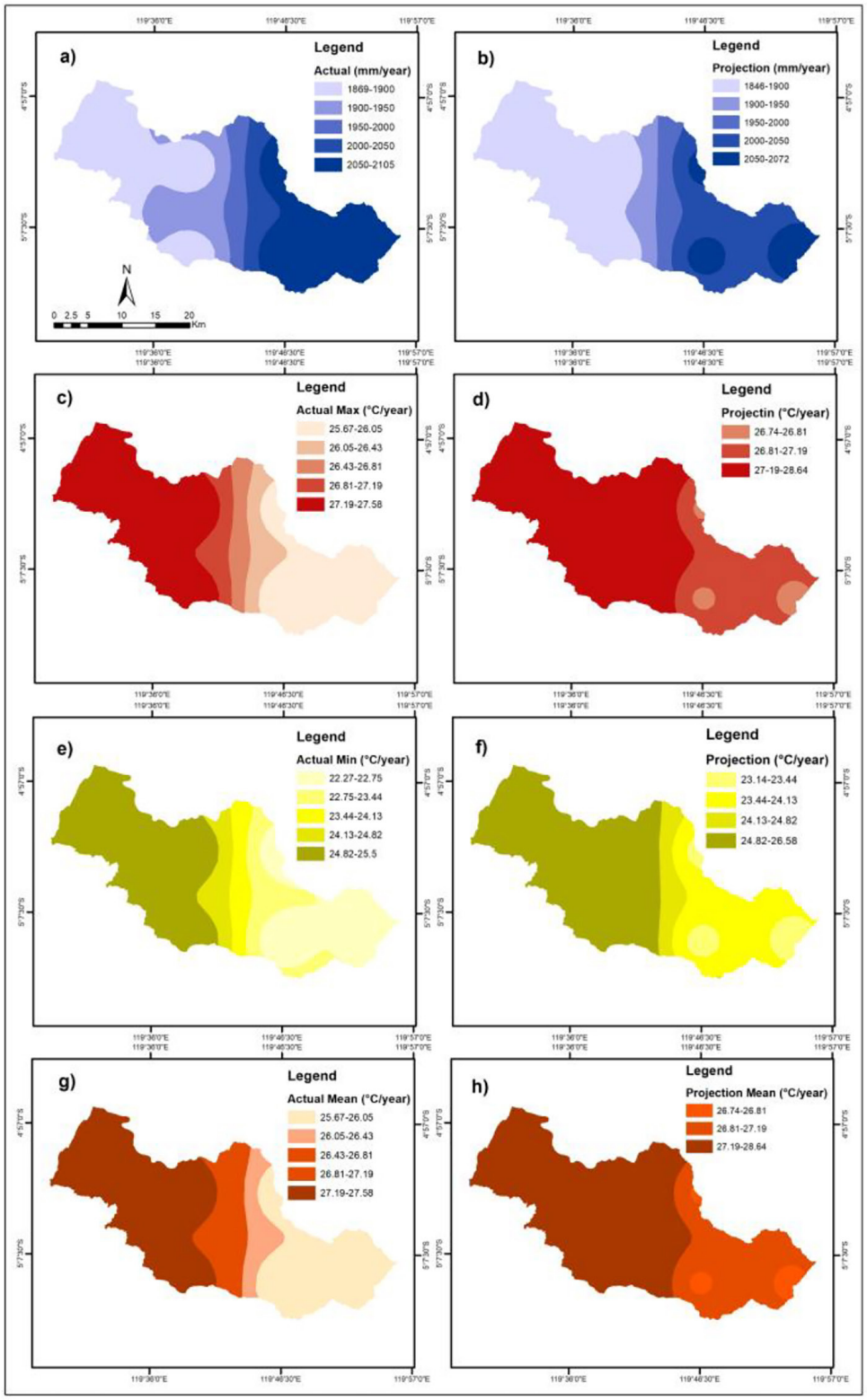

Figure 6. Spatial analysis of actual and climate projections for the Maros Watershed. a) Actual precipitation; b) projected precipitation; c) actual maximum temperature; d) projected maximum temperature; e) actual minimum temperature; f) projected minimum temperature; g) actual mean temperature; h) projected mean temperature

Other classes, such as secondary mangrove forests, savannas, shrublands, open land, and water, were relatively stable, with minor changes. The transport sector, that is, airports, tends to be stable, which shows that the main infrastructure has been formed since 2014.

Table 2. Land cover data from 2014, 2019 and 2023 in the Maros watershed

Land cover	Area in 2014		Area in 2019		Area in 2023		Change area (2014–2023)	
	ha	%	ha	%	ha	%	ha	ha/year
Airport area	380.12	0.53	380.12	0.53	380.12	0.53	0.00	0.00
Secondary forest	28,663.56	39.62	27,067.56	37.41	25,223.95	34.86	-3,439.61	-382.18
Secondary mangrove forest	320.43	0.44	299.78	0.41	285.59	0.39	-34.84	-3.87
Planted forest	1,976.74	2.73	2,077.08	2.87	1,985.24	2.74	8.50	0.94
Settlement	2,511.33	3.47	2,894.35	4.00	3,811.65	5.27	1,300.32	144.48
Agricultural/crop land	7,006.23	9.68	9,235.04	12.76	9,595.94	13.26	2,589.71	287.75
Mixed agricultural/agroforestry	9,474.98	13.10	8,393.67	11.60	8,179.10	11.31	-1,295.88	-143.99
Grassland	511.44	0.71	545.09	0.75	529.15	0.73	17.71	1.97
Paddy area	12,960.86	17.91	12,779.17	17.66	14,007.22	19.36	1,046.36	116.26
Shurbland	1,279.41	1.77	1,250.85	1.73	1,321.55	1.83	42.14	4.68
Fish pond	6,001.75	8.30	5,934.42	8.20	5,723.20	7.91	-278.54	-30.95
Open area	497.46	0.69	752.66	1.04	539.43	0.75	41.98	4.66
Water	764.65	1.06	739.17	1.02	766.81	1.06	2.16	0.24
Total area	72,348.95	100	72,348.95	100	72,348.95	100		

Land cover changes at the research site occurred in a fluctuating manner, particularly in the secondary forest class. The decrease in the area of this class is due to the agricultural activities of the community, which are aimed at meeting the food economy needs of the region. This is in line with the implementation of national policies related to food security (Arifanti et al., 2021; Putra et al., 2019). In addition, increasing demographic pressures are driving the development of residential and infrastructure areas in the Mamminasata Metropolitan Area. Given that the study location is in a hilly topographic zone with a predominance of steep slope classes, land conversion in this area increases the region's vulnerability index to geophysical disasters, such as landslides and floods, and triggers massive erosion and sedimentation rates (Rahmat et al., 2023; Soma et al., 2023; Soma and Kubota, 2017) (Table 3).

According to the spatial simulations that have been validated, it is quite "good" (Kappa accuracy of 76.41%), and the land cover of the Maros watershed in 2064 is expected to continue

Table 3. Projected land cover data for 2064 in the Maros watershed

Land cover	Area in 2023		Area in 2064		Change area (2023–2064)	
	ha	%	ha	%	ha	ha/year
Airport area	380.12	0.53	380.79	0.53	0.67	0.13
Secondary forest	25,223.95	34.86	24,971.90	34.52	-252.05	-50.41
Secondary mangrove forest	285.59	0.39	260.52	0.36	-25.07	-5.01
Planted forest	1,985.24	2.74	1,985.30	2.74	0.06	0.01
Settlement	3,811.65	5.27	3,932.19	5.44	120.54	24.11
Agricultural/crop land	9,595.94	13.26	9,727.18	13.44	131.24	26.25
Mixed agricultural/agroforestry	8,179.10	11.31	8,171.49	11.29	-7.61	-1.52
Grassland	529.15	0.73	526.45	0.73	-2.70	-0.54
Paddy area	14,007.22	19.36	14,009.92	19.36	2.70	0.54
Shurbland	1,321.55	1.83	1,324.26	1.83	2.71	0.54
Fish pond	5,723.20	7.91	5,748.24	7.95	25.03	5.01
Open area	539.43	0.75	540.67	0.75	1.24	0.25
Water	766.81	1.06	770.05	1.06	3.23	0.65
Total area	72,348.95	100	72,348.95	100		

to be dominated by pressure on forest areas. The deforestation rate of secondary forests was recorded at 50.41 ha/year, inversely proportional to the increase of 24.11 ha in settlement and agricultural areas. A change in the characteristics of the ground surface to become more impermeable will inhibit soil infiltration. This condition, when contrasted with the trend of high annual precipitation, has the potential to increase the volume of surface runoff, thus indicating a high level of vulnerability to the risk of floods and other hydrometeorological disasters in the future. The expansion of agriculture/crop land (26.25 ha/year) in upstream or sloping areas, if not managed with good conservation, can trigger further erosion, as the precipitation intensity in the Maros watershed peaks in January (Kayitesi et al., 2022; Siyamsih, 2024) (Figure 7).

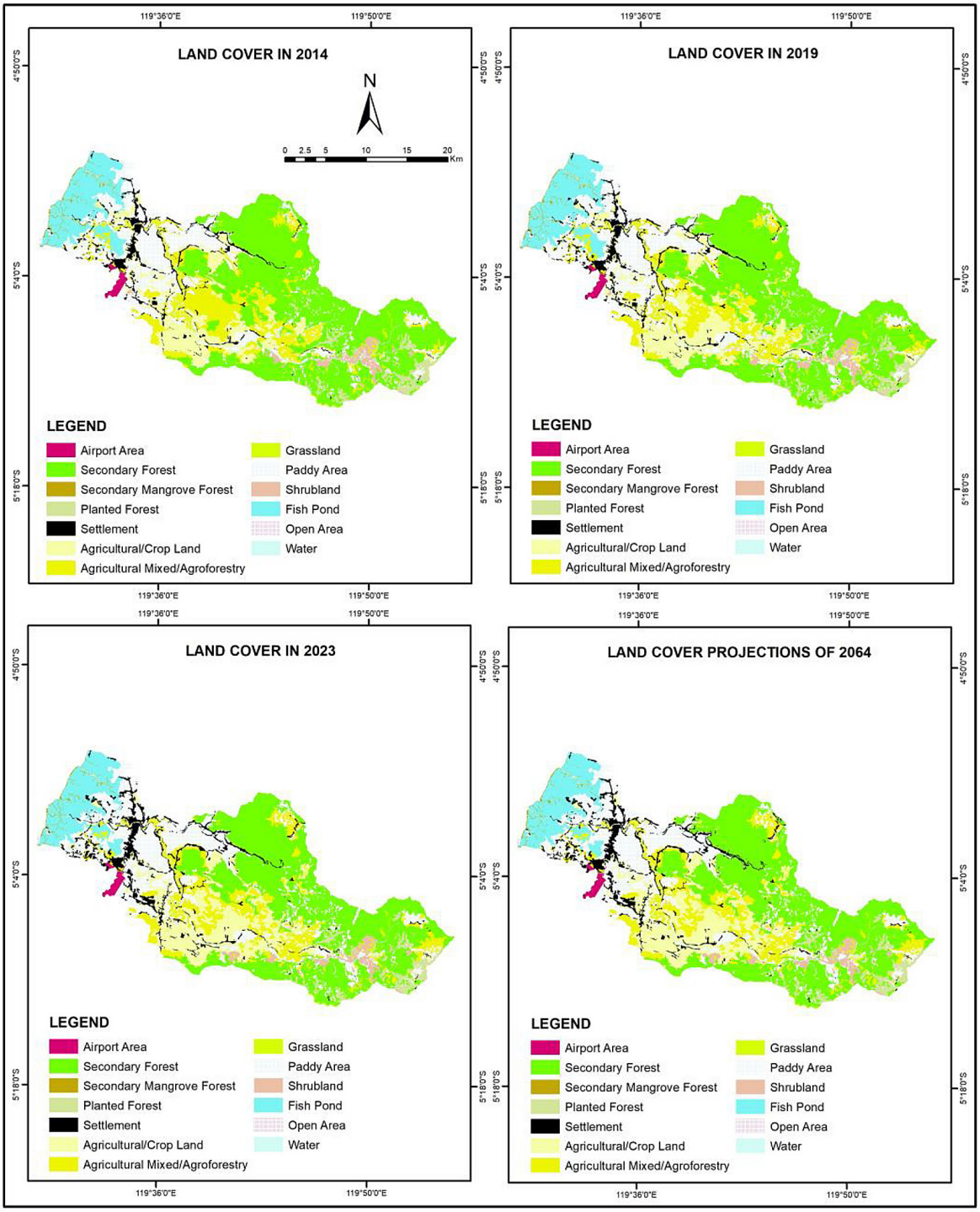

Figure 7. Spatial land cover data for 2014, 2019, and 2023 and 2064 projections for the Maros watershed

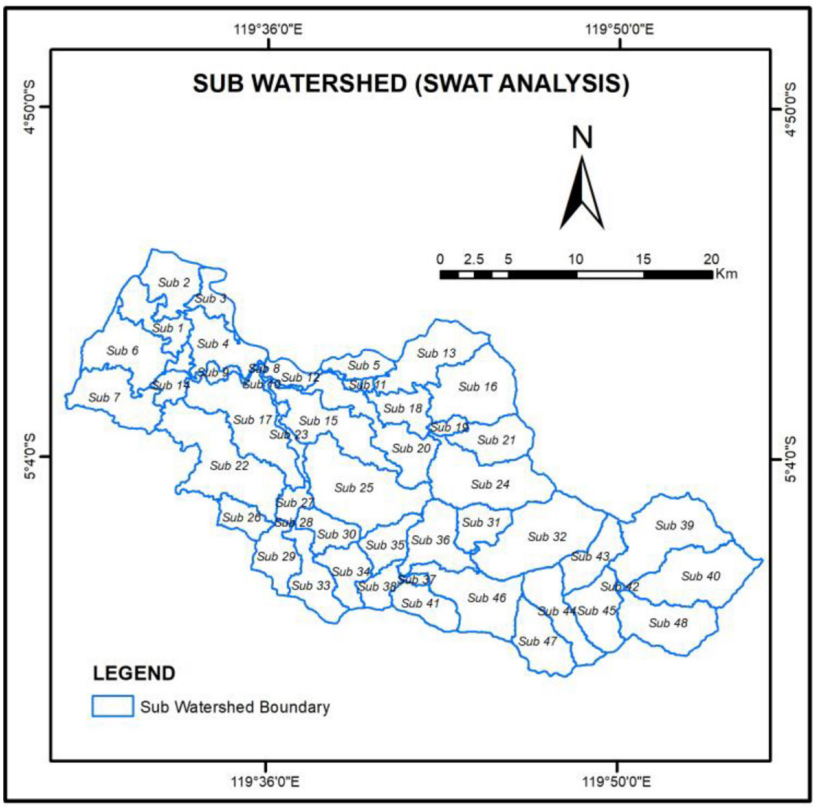

Figure 8. Subwatershed from the SWAT analysis in the Maros watershed

Watershed deliniation and HRU establishment

Using the DEM input data, spatial delimitation was performed to define the catchment area and river network. On the basis of the determination of the direction and accumulation of flow, the watershed was divided into 48 subwatersheds (Figure 8). Within the SWAT framework, this spatial structure is detailed in the HRU. The HRU represents the smallest unit of analysis with uniform hydrological characteristics, resulting

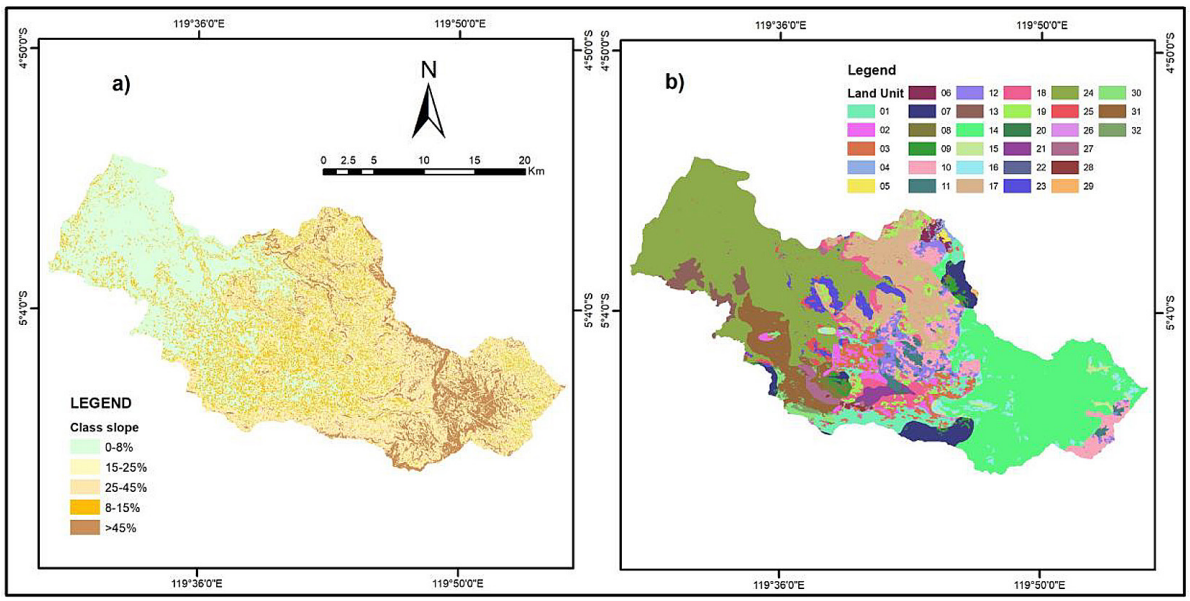

Figure 9. a) Class slope; b) land unit

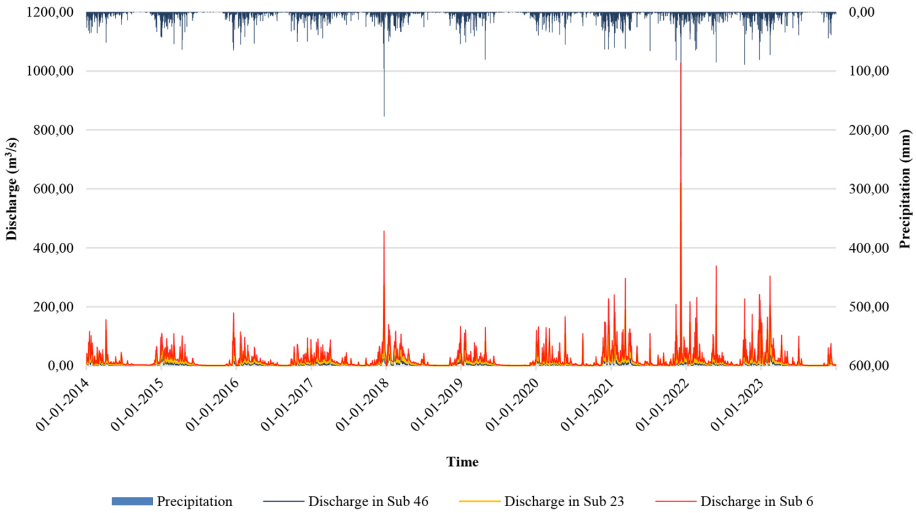

Figure 10. Daily discharge data (2014–2023) for subwatersheds 46, 23, and 6

from the overlay of land cover, soil, and topographic parameters.

The variations in land cover, soil, and slope (Figure 9) were combined in each HRU to allow hydrological simulation in a hydrologically homogeneous area. According to the training results, there was a variation in the number of HRUs in each scenario: 3.234 units (2014), 3.419 units (2019), and 3.278 units (2023), which increased to 3.475 units for the 2064 projection. With this splitting mechanism, the SWAT model can more accurately calculate surface flow, infiltration, evapotranspiration, and discharge based on the different conditions of each HRU.

SWAT results

In this study, SWAT demonstrated its ability to calculate discharge in the Maros watershed. In this analysis, the data range used is the daily data range. During the period of 2014–2023, the simulation SWAT results in Figure 10 reveal a significant relationship between precipitation intensity and flow fluctuations in the three watershed representation zones (upstream in subwatershed 46, middle in subwatershed 23, and downstream in subwatershed 6). The extreme rainfall event of December 7, 2021, caused the highest peak flow, reaching 1.206 m^3/s in subwatershed 6, 618.70 m^3/s in subwatershed 23, and 289.80 m^3/s in subwatershed 46. The difference in flow values between the upstream and downstream areas reflects the heterogeneity of the catchment area in each HRU. The HRU is illustrated by the physical conditions of the soil and slopes, as well as by land cover changes.

In addition, projected daily discharge data for 2064 show that each sub watershed has an increase in discharge value from December to April, with peak conditions occurring on February 13, with flows of 184.10 m^3/s in sub watershed 6, 133 m^3/s in sub watershed 23, and 79.40 m^3/s in sub watershed 46. Steep slopes and high amounts of precipitation produce a hydrological response, with rapid and high increases in river flow caused by morphological conditions, intense rainfall, and changes in land cover that reduce water storage and infiltration capacity (Borsos and Sendzimir, 2018; Dehaspe et al., 2018). Therefore, the response of the river to high rainfall is very rapid, with an increase in flow.

A comparison of the period of 2014–2023 with the projection for 2064 revealed a change in the hydrological cycle of the Maros watershed in a more extreme direction. Although the discharge value in the 2064 scenario was low, the duration of the absence of flow in the dry season was expected to be much longer. This phenomenon aggravates the vulnerability of watersheds, reinforcing indications of a reduction in secondary dryland forests by 50.41 ha/year due to agricultural and settlement expansion, which affects regional water absorption. As a result, rivers lose their natural ability to maintain base flow, triggering the risk of hydrological droughts in the dry season and flooding in more severe rainy seasons (Qi et al., 2020; Wang et al., 2013) (Figure 11).

To validate the SWAT simulation results, model parameter optimization was performed through repeated calibrations to ensure the precision or goodness of fit between the simulation

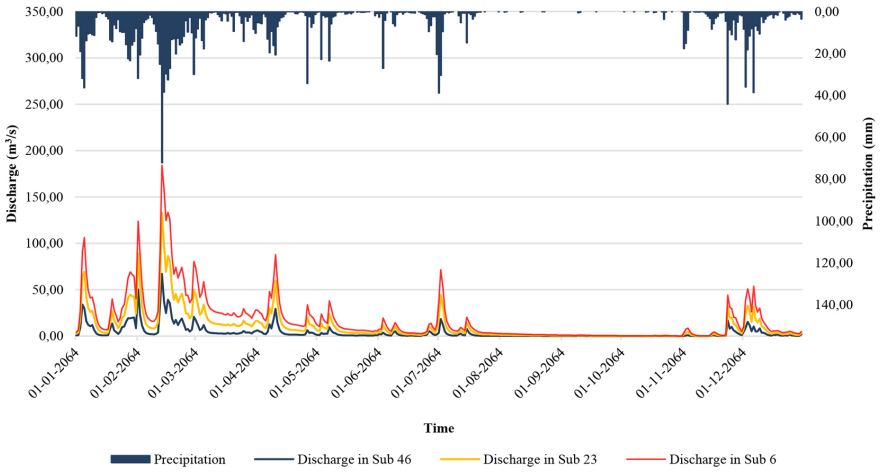

Figure 11. Daily discharge data (2064) for subwatersheds 46, 23, and 6

Table 4. SWAT calibration parameters

No	Parameter	File extention	Fitted value	Min value	Max value
1	R_CN2	mgt	0.96	-0.20	1.00
2	V_ALPHA_BF	gw	0.15	0.00	1.00
3	V_GW_DELAY	gw	32.50	0.00	500.00
4	R_GWQMN	gw	475.00	0.00	5000.00
5	R_SURLAG	bsn	6.47	0.05	10.00

Table 5. SWAT validation results

Simulasi	Simulation period	R^2	NSE
Pra-Kalibrasi Batubassi	2010-2014	0.52	0.14
Pra-Kalibrasi Lekopancing	2010-2014	0.71	0.59
Validasi Batubassi	2015-2019	0.6	0.5
Validasi Lekopancing	2015-2019	0.71	0.75
Validasi Batubassi	2020-2023	0.48	0.42
Validasi Lekopancing	2020-2023	0.72	0.65

discharge and observation. Calibration and validation tests were performed on two sets of flow observation data, namely, Lekopancing and Batubassi Dams data. The obstacles faced by this study were the existence of some missing data or the absence of daily data. Daily tests are rated poorly and are performed with monthly average data. This evaluation is quite good and can be performed in the evaluation of models (Hermawan et al., 2025). The parameters used for calibration are listed in Table 4.

The final results of the evaluation of the existing simulation are presented in Table 5.

The results of the model validation revealed a difference in the statistical performance between the two observational datasets. The validation results revealed the best evaluation of the Lekopaccing Dam, with an R^2 value of > 0.71 and an NSE in the range of 0.49–0.75. This evaluation is in the "Decent" and "Satisfactory" categories, with the highest NES in the period 2015–2019. However, the lower accuracy at Batubassi Dam was due to the incompleteness of the available input data series. However, taken together, the R^2 and NSE values obtained are still within the acceptable range for long-term prediction purposes, especially since the study simulates hydrological interactions due to climate variability and land cover change in the study area (Figure 12).

Figure 12. Relationships between the observed and simulated discharges during the validation period from 2010–2023

CONCLUSIONS

This study successfully applied an integrated modeling framework to quantify the impacts of land-cover transformation and climate variability on discharge dynamics in the rapidly urbanizing tropical karst Maros watershed. Overall, the SWAT model showed a satisfactory level of accuracy in representing the dose-response to rainfall and land cover, despite variability in model performance owing to the availability of observational data. Based on the formulated hypotheses, the spatial and hydrological analyses revealed several key findings. First (H1), significant and consistent changes in land cover, characterized by the continued rate of deforestation of secondary forests and the massive expansion of agricultural land and settlements, have led to the expansion of impermeable surfaces, which has directly increased peak discharge and altered base flows. Second (H2), climate projections indicating fluctuating rainfall patterns have amplified seasonal discharge variability. Third (H3), the combined effects of land cover and climate change have directly resulted in a rapid and amplified response between extreme precipitation events and discharge surges. Finally (H4), the hydrological responses exhibited strong spatial heterogeneity, as evidenced by the varying simulated maximum flows across different subwatersheds depending on their local sensitivities. These findings emphasize the necessity of integrating dynamic land-use planning with climate adaptation strategies to mitigate future hydrological extremes in the region.

REFERENCES

1. Akoko, G., Le, T. H., Gomi, T., Kato, T. (2021). A review of SWAT model application in Africa. *Water, 13*(1313), 1–20. https://doi.org/10.3390/w13091313
2. Aprizal, Meris, A. (2020). Aplikasi Hec-Ras dalam Pengendalian Banjir Sungai Way Kandis - Lampung Selatan. *Jurnal Teknik Sipil ITP, 7*(1), 1–9. https://doi.org/10.21063/jts.2019.v701.01
3. Arifanti, V. B., Novita, N., Subarno, Tosiani, A. (2021). Mangrove Deforestation and CO_2 Emissions in Indonesia. *IOP Conference Series: Earth and Environmental Science, 874*(012006), 1–10. https://doi.org/10.1088/1755-1315/874/1/012006
4. Borsos, B., Sendzimir, J. (2018). *The Tisza River: Managing a Lowland River in the Carpathian Basin.* Springer, 541–560. https://doi.org/10.1007/978-3-319-73250-3
5. Cordeiro, M. R. C., Wilson, H. F., Vanrobaeys, J., Pomeroy, J. W., Fang, X. (2017). Simulating cold-region hydrology in an intensively drained agricultural watershed in Manitoba, Canada, using the cold regions hydrological model. *Hydrology and Earth System Sciences, 21*(7), 3483–3506. https://doi.org/10.5194/hess-21-3483-2017
6. Dehaspe, J., Birkel, C., Tetzlaff, D., Murillo, R. S., María, A., Quesada, D., Soulsby, C. (2018). Spatially distributed tracer ‐ aided modeling to explore water and isotope transport, storage and mixing in a pristine, humid tropical catchment. *Hydrological Processes, 32*(21), 3206–3224. https://doi.org/10.1002/hyp.13258
7. Djafar, M., Faisal, M. (2019). Strategi pengembangan ekowisata karst di Dusun Rammang-Rammang Maros, Sulawesi Selatan. *Gorontalo Journal of Forestry Research, 2*(1), 1–9. https://doi.org/10.32662/gjfr.v2i1.498
8. Dwivedi, S. K., Thakur, P. K., Dhote, P. R., Kruczkiewicz, A., Upadhyay, M., Moothedan, A. J., Bisht, M., Singh, R. P. (2024). Unraveling flash flood dynamics of song watershed, Doon Valley: Key insights for floodplain management. *Geomatics, Natural Hazards and Risk, 15*(1). https://doi.org/10.1080/19475705.2024.2378979
9. Faqih, A. (2017). A Statistical Bias Correction Tool for Generating Climate Change Scenarios in Indonesia based on CMIP5. *IOP Conference Series: Earth and Environmental Science, 58*(1), 1–12. https://doi.org/10.1088/1755-1315/5
10. Farjad, B., Gupta, A., Marceau, D. J. (2016). Annual and seasonal variations of hydrological processes under climate change scenarios in two sub-catchments of a complex watershed. *Water Resources Management, 30*(8), 2851–2865. https://doi.org/10.1007/s11269-016-1329-3
11. Farzana, S. Z., Zafor, A., Shahariar, J. Al. (2019). Application of SWAT model for assessing water availability in Surma River Basin. *Jurnal of The Civil Engineering Forum, 5*(1), 29–38. https://doi.org/10.22146/jcef.39191
12. Gelaro, R., McCarty, W., Suárez, M. J., Todling, R., Molod, A., Takacs, L., Randles, C. A., Darmenov, A., Bosilovich, M. G., Reichle, R., Wargan, K., Coy, L., Cullather, R., Draper, C., Akella, S., Buchard, V., Conaty, A., da Silva, A. M., Gu, W., … Zhao, B. (2017). The modern-era retrospective analysis for research and applications, version 2 (MERRA-2). *Journal of Climate, 30*(14), 5419–5454. https://doi.org/10.1175/JCLI-D-16-0758.1
13. Golmohammadi, G., Prasher, S., Madani, A., Rudra, R. (2014). Evaluating three hydrological distributed watershed models: MIKE-SHE, APEX, SWAT. *Hydrology, 1*(1), 20–39. https://doi.org/10.3390/hydrology1010020
14. Hasan, M. A., Pradhanang, S. M. (2017). Estimation of flow regime for a spatially varied himalayan watershed using improved multi-site calibration of the soil and water assessment tool (SWAT) model. *Environment Earth Scince, 76*(787), 1–13. https://doi.org/10.1007/s12665-017-7134-3
15. Hayati, N., Wakka, A. K. (2016). Valuasi ekonomi manfaat air di Taman Nasional Bantimurung Bulusaraung, Sulawesi Selatan. *Jurnal Penelitian Sosial Dan Ekonomi Kehutanan, 13*(1), 47–61. https://doi.org/10.20886/jpsek.2016.13.1.47-61
16. Hermawan, S. G., Suprayogi, S., Fadlillah, L. N. (2025). Soil and water assessment tool (SWAT) model for hydrological response analysis in the Gajahwong Subwatershed, Yogyakarta, Indonesia. *Journal Od Degraded and Mining Lands Management, 12*(2), 7297–7299. https://doi.org/10.15243/jdmlm.2025.122.7297
17. Huang, A. T., Gillet, Z. E., Taschetto, A. S. (2024). Australian rainfall increases during multi ‐ year La Niña. *Geophysical Research Letters, 51*(9), 1–10. https://doi.org/10.1029/2023GL106939
18. Huang, C., Zhang, Y., Hou, J. (2024). Soil and water assessment tool (SWAT)-informed deep learning for streamflow forecasting with remote sensing and in situ precipitation and discharge observations. *Remote Sensing, 16*(3999), 1–22. https://doi.org/10.3390/rs16213999
19. Hyandye, C. B., Worqul, A., Martz, L. W., Muzuka, A. N. N. (2018). The impact of future climate and land use/cover change on water resources in the Ndembera Watershed and their mitigation and adaptation strategies. *Environmental Systems Research, 7*(7), 1–24. https://doi.org/10.1186/s40068-018-0110-4
20. Islami, F. A., Tarigan, S. D., Wahjunie, E. D., Dasanto, B. D. (2022). Accuracy Assessment of Land Use Change Analysis Using Google Earth in Sadar Watershed Mojokerto Regency Accuracy Assessment of Land Use Change Analysis Using

Google Earth in Sadar Watershed Mojokerto Regency. *IOP Conference Series: Earth and Environmental Science, 950*(1), 012091. https://doi.org/10.1088/1755-1315/950/1/012091

21. Kayitesi, N. M., Guzha, A. C., Mariethoz, G. (2022). Impacts of land use land cover change and climate change on river hydromorphology- A review of research studies in tropical regions. *Journal of Hydrology, 615*(128702), 1–14. https://doi.org/10.1016/j.jhydrol.2022.128702
22. Kibii, J. K., Kipkorir, E. C., Kosgei, J. R. (2021). Application of soil and water assessment tool (SWAT) to evaluate the impact of land use and climate variability on the Kaptagat Catchment River discharge. *Sustainability, 13*(1802), 1–19. https://doi.org/10.3390/su13041802
23. Knighton, J. O., Degaetano, A., Walter, M. T. (2017). Hydrologic state influence on riverine flood discharge for a small temperate watershed (Fall Creek, United States): Negative feedbacks on the effects of climate change. *Journal of Hydrometeorology, 18*(2), 431–449. https://doi.org/10.1175/JHM-D-16-0164.1
24. Kumar, M., Denis, D. M., Kundu, A., Joshi, N., Suryavanshi, S. (2022). Understanding land use/land cover and climate change impacts on hydrological components of Usri Watershed, India. *Applied Water Science, 12*(39), 1–14. https://doi.org/10.1007/s13201-021-01547-6
25. Liu, Z., Cuo, L., Li, Q., Liu, X., Ma, X., Liang, L., Ding, J. (2020). Impacts of climate change and land use/cover change on streamflow in Beichuan River Basin in Qinghai Province, China. *Water, 12*(1198), 1–26. https://doi.org/10.3390/w12041198
26. Malede, D. A., Alamirew, T., Andualem, T. G. (2023). Integrated and individual impacts of land use land cover and climate changes on hydrological flows over Birr River. *Water, 15*(166), 1–22. https://doi.org/10.3390/w15010166
27. Mathewos, M., Lencha, S. M., Tsegaye, M. (2022). Land use and land cover change assessment and future predictions in the Matenchose Watershed, Rift Valley Basin, using CA-Markov simulation. *Land, 11*(1632), 1–28. https://doi.org/10.3390/land11101632
28. McGregor, J. L., Nguyen, K. C., Kirono, D. G. C., Katzfey, J. J. (2016). High-resolution climate projections for the islands of Lombok and Sumbawa, Nusa Tenggara Barat Province, Indonesia. *Challenges and Implications. Climate Risk Management, 12*, 32–44. https://doi.org/http://dx.doi.org/10.1016/j.crm.2015.10.001
29. Mollel, G. R., Mulungu, D. M. M., Nobert, J., Alexander, A. C. (2023). Assessment of climate change impacts on hydrological processes in the Usangu Catchment of Tanzania Under CMIP6 scenarios. *Journal of Water and Climate Change, 14*(11), 4162–4182. https://doi.org/10.2166/wcc.2023.542
30. Moura, L. B., Lopes, T. R., Duarte, S. N., Sica, P., Folegatti, M. V. (2025). Hydrological assessment using the SWAT model in the Jundiaí River Basin, Brazil: Calibration, model performance, and land use change impact analysis. *Resources, 14*(112), 1–24. https://doi.org/10.3390/resources14070112
31. Pratomoatmojo, N. A. (2018a). LanduseSim Algorithm: Land Use Change Modeling by Means of Cellular Automata and Geographic Information System. *IOP Conference Series: Earth and Environmental Science-CITIES2017, 202*(012020), 1–13. https://doi.org/10.1088/1755-1315/202/1/012020
32. Pratomoatmojo, N. A. (2018b). LanduseSim Methods: Land Use Class Hierarchy for Simulations of Multiple Land Use Growth. *IOP Conference Series: Earth and Environmental Science-CITIES2017, 202*(012023), 1–9. https://doi.org/10.1088/1755-1315/202/1/012023
33. Pratomoatmojo, N. A. (2018c). Permodelan perubahan penggunaan lahan berbasis cellular automata dan sistem informasi geografis dengan menggunakan LanduseSim. *Jurnal Penataan Ruang, 13*(1), 26. https://doi.org/10.12962/j2716179x.v13i1.7064
34. Pregnolato, M., Ford, A., Wilkinson, S. M., Dawson, R. J. (2017). The impact of flooding on road transport: a depth-disruption function. *Transportation Research Part D, 55*, 67–81. https://doi.org/10.1016/j.trd.2017.06.020
35. Putra, A. H., Oktari, F., Putriana, A. M. (2019). Deforestasi dan pengaruhnya terhadap tingkat bahaya kebakaran hutan di kabupaten Agam Provinsi Sumatera Barat. *Jurnal Dialog Penanggulangan Bencana, 10*(2), 191–200. https://jdpb.bnpb.go.id/index.php/jurnal/article/view/143
36. Qi, P., Xu, Y. J., Wang, G. (2020). Quantifying the individual contributions of climate change, dam construction, and land use/land cover change to hydrological drought in a Marshy River. *Sustainability, 12*(19), 3777. https://doi.org/10.3390/su12093777
37. Rahmat, S., Soma, A. S., Barkey, R. A. (2023). Land Cover Changes In Bila Watershed, South Sulawesi, Indonesia. *IOP Conf. Series: Earth and Environmental Sciene-FSSAT-4, 1230*(012045), 1–10. https://doi.org/10.1088/1755-1315/1230/1/012045
38. Rajaei, F., Sari, A. E., Salmanmahiny, A., Delavar, M., Bavani, A. R. M., Srinivasan, R. (2016). Surface drainage nitrate loading estimate from agriculture fields and its relationship with landscape metrics In Tajan Watershed. *Paddy and Water Environment, 15*, 541–554. https://doi.org/10.1007/s10333-016-0570-y
39. Rotstayn, L. D., Jeffrey, S. J., Collier, M. A., Dravitzki, S. M., Hirst, A. C., Syktus, J. I., Wong, K. K. (2012). Aerosol-and greenhouse gas-induced changes in summer rainfall and circulation in the Australasian Region: A study using single-forcing

climate simulations. *Atmospheric Chemistry and Physics, 12*(14), 6377–6404. https://doi.org/10.5194/acp-12-6377-2012

40. Siyamsih, D. (2024). Impacts of deforestation on soil quality and water resources in tropical forest areas of Sumatra. *Journal of Horizon, 1*(1), 16–22. https://doi.org/10.62872/kvmcwq82
41. Soma, A. S., Arsyad, U., Nursaputra, M., Lando, A. T., Rahmat, S., Azus, F. H., Ramadhan, M. D. R. (2023). Flood Vulnerability Analysis Using The Frequency Ratio Method with The Watershed Ecosystem in Bulukumba Regency, South Sulawesi Indonesia. *IOP Conf. Series: Earth and Environmental Sciene-FSSAT-4, 1230*(012044), 1–7. https://doi.org/10.1088/1755-1315/1230/1/012044
42. Soma, A. S., Kubota, T. (2017). The performance of land use change causative factor on landslide susceptibility map in Upper Ujung-Loe Watersheds South Sulawesi, Indonesia. *Geoplanning: Journal of Geomatics and Planning, 4*(2), 157–170. https://doi.org/10.14710/geoplanning.4.2.157-170
43. Suhairin. (2020). Evaluasi kemampuan lahan untuk arahan penggunaan lahan di daerah aliran sungai Maros Sulawesi Selatan. *Jurnal Agrotek, 7*(1), 50–58. https://doi.org/10.31764/agrotek.v7i1.2352
44. Sulmiah, Sakawati, H., Widyawati, Rukmana, N. S. (2019). Analisis kebijakan pembangunan kawasan metropolitan di Indonesia Timur: Dampak terhadap tata kelola perkotaan. *Jurnal Ilmu Administrasi: Media Pengembangan Ilmu Dan Praktek Administrasi, 16*(2), 258–272. https://doi.org/10.31113/jia.v16i2.519
45. Supari, Tangang, F., Salimun, E., Aldrian, E., Sopaheluwakan, A., Juneng, L. (2017). ENSO modulation of seasonal rainfall and extremes in Indonesia. *Climate Dynamics, 51*(7–8), 2559–2580. https://doi.org/10.1007/s00382-017-4028-8
46. Surya, B., Muhibuddin, A., Suriani, S., Rasyidi, E. S., Baharuddin, B., Fitriyah, A. T., Abubakar, H. (2021). Economic evaluation, use of renewable energy, and sustainable urban development Mamminasata Metropolitan, Indonesia. *Sustainability, 13*(1165), 1–45. https://doi.org/10.3390/su13031165
47. Talib, A., Randhir, T. O. (2017). Climate change and land use impacts on hydrologic processes of watershed systems. *Journal of Water and Climate Change, 8*(3), 363–374. https://doi.org/10.2166/wcc.2017.064
48. Tangang, F., Chung, J. X., Juneng, L., Supari, Salimun, E., Ngai, S. T., Jamaludin, A. F., Mohd, M. S. F., Cruz, F., Narisma, G., Santisirisomboon, J., Ngoh-Duc, T., Tan, P. Van, Singhruck, P., Gunawan, D., Aldrian, E., Sopaheluwakan, A., Grogory, N., Remedio, A. R. C., … Kumar, P. (2020). Projected future changes in rainfall in Southeast Asia based on CORDEX–SEA multi-model simulations. *Climate Dynamics, 55*(5), 1247–1267. https://doi.org/10.1007/s00382-020-05322-2
49. Tilahun, A., Teferie, B. (2015). Accuracy assessment of land use land cover classification using google earth. *America Journal of Environmental Protection, 4*(4), 193–198. https://doi.org/10.11648/j.ajep.20150404.14
50. Ummenhofer, C. C., Gupta, A. Sen, England, M. H., Taschetto, A. S., Briggs, P. R., Raupach, M. R. (2015). How did ocean warming affect Australian rainfall extremes during the 2010/2011 La Niña event? *Geophysical Research Letters, 42*(22), 9942–9951. https://doi.org/10.1002/2015gl065948
51. Upadhyay, P., Linhoss, A., Kelble, C., Ashby, S., Murphy, N., Parajuli, P. B. (2022). Applications of the SWAT model for coastal watersheds: Review and recommendations. *Journal of the ASABE, 65*(2), 453–469. https://doi.org/10.13031/ja.14848
52. Wang, R., Kalin, L., Kuang, W., Tian, H. (2013). Individual and combined effects of land use/cover and climate change on wolf bay watershed stream flow in Southern Alabama. *Hydrological Processes, 28*(22), 5530–5546. https://doi.org/10.1002/hyp.10057
53. Wang, Y., Jiang, R., Xie, J., Zhao, Y., Yan, D., Yang, S. (2019). Soil and water assessment tool (SWAT) model: A systemic review. *Journal of Coastal Research, 93*, 22–30. https://doi.org/10.2112/si93-004.1
54. Wldmchel, M., Osore, A. (2025). Evaluation of the impact of climate and land use/land cover change on hydrological response in Gelna Watershed. *PLOS Climate, 4*(1), 1–27. https://doi.org/10.1371/journal. pclm.0000483
55. Xie, S., Zhu, Y. (2022). Prediction of the discharge flow in a small hydropower station without hydrological data based on SWAT model. *Water (Switzerland), 14*(13). https://doi.org/10.3390/w14132011
56. Xu, H., Taylor, R. G., Kingston, D. G., Jiang, T., Thompson, J. R., Todd, M. C. (2010). Hydrological modeling of River Xiangxi using SWAT2005: A comparison of model parameterizations using station and gridded meteorological observations. *Quaternary International, 226*(1–2), 54–59. https://doi.org/10.1016/j.quaint.2009.11.037
57. Yanuar, M. A., Dewi, R. S., Handayani, W. (2023). Perkembangan Metropolitan Mamminasata: Tinjauan kesenjangan aspek sosial-ekonomi dan tata Kelola wilayah. *Region: Jurnal Pembangunan Wilayah Dan Perencanaan Pasrtisipatif, 18*(1), 194–209. https://doi.org/10.20961/region.v18i1.60006
58. Zhong, X., Xu, Q., Yi, J., Jin, L. (2022). Study on the threshold relationship between landscape pattern and water quality considering spatial scale effect – A case study of Dianchi Lake Basin In China. *Environmental Science and Pollution Research, 29*, 44103–44118. https://doi.org/10.1007/s11356-022-18970-0